Die Pharmazie

Pharmazie **2026**; 81(8): 54200
https://doi.org/10.31083/Pharmazie54200

Research Article

The Active Fraction From *Polyporus umbellatus* Against Hyperuricemia

Jian Luo[1,2,†], Xin-yu Chen[2,3,†], Run-ze Jin[3], Si-yao Zhang[3], Meng-qi Zhou[3], Yun-yan Chen[3], Yu Sun[3], Dao-yin Yang[3], Xiao-wen Gong[3], Jian-hao Xu[3], Si-hui Nian[2,3,*], Ling-yun Zhou[2,3,*]

[1]Market Regulation Bureau in Lujiang County, 231500 Lujiang, Anhui, China
[2]Provincial Engineering Laboratory for Screening and Reevaluation of Active Compounds of Herbal Medicines in Southern Anhui, 241002 Wuhu, Anhui, China
[3]College of Pharmacy, Wannan Medical University, 241002 Wuhu, Anhui, China
*Correspondence: niansihui@126.com (Si-hui Nian); zly4321@sina.com (Ling-yun Zhou)
[†]These authors contributed equally.
Academic Editors: Mattia Mori and Walter E. Müller
Submitted: 24 May 2026 Revised: 6 July 2026 Accepted: 15 July 2026 Published: 21 August 2026

Abstract

Objective: This study aimed to identify the active fraction of *Polyporus umbellatus* extract (PUE) for the treatment of hyperuricemia (HUA) and elucidate the associated mechanism of action. **Methods:** HUA was induced in mice using hypoxanthine and potassium oxonate. Serum uric acid (UA), urinary UA, creatinine (CRE), blood urea nitrogen (BUN), xanthine oxidase (XOD) activity, inflammatory cytokines (Interleukin-6 (IL-6), Tumor necrosis factor-α (TNF-α)), and renal urate transporters (Uric acid transporter 1 (URAT1), Organic anion transporter 1 (OAT1)) were subsequently measured. The active fraction was identified by bioactivity-guided fractionation using D101 macroporous resin chromatography. Two major compounds were isolated and evaluated for anti-inflammatory (nitric oxide (NO) production, cytokine mRNA expression) and antioxidant (Malondialdehyde (MDA), Superoxide dismutase (SOD)) activities in monosodium urate (MSU)-induced RAW264.7 macrophages. **Results:** PUE significantly ameliorated hyperuricemia in HUA mice, reducing serum UA, CRE, BUN, and renal URAT1 expression; increasing urinary UA excretion and OAT1 expression; inhibiting XOD activity; attenuating renal inflammation and histopathological damage. The 95% ethanol eluate was identified as the most active fraction and yielded ergosterol (A) and 5α,8α-epidioxy-(22E,24R)-ergosta-6,22-dien-3β-ol (B). Both compounds suppressed MSU-induced NO release, proinflammatory cytokine expression, and oxidative stress. **Conclusion:** The 95% ethanol eluate of *P. umbellatus* exerts anti-hyperuricemic effects through multiple mechanisms, possibly related to XOD inhibition, anti-inflammatory activity, antioxidant protection, and regulation of renal uric acid transport proteins. Ergosterol derivatives are proposed as the potential active components in this extract.

Keywords: *Polyporus umbellatus*; hyperuricemia; the active fraction

1. Introduction

Hyperuricemia (HUA) is a widespread metabolic disturbance characterized by abnormally high serum uric acid (UA) concentrations, with a steadily rising prevalence across populations worldwide [1]. Long-standing HUA confers increased susceptibility to nephropathy, cardiovascular events, and attendant clinical sequelae [2]. HUA can also cause gouty arthritis. Current anti-gout drugs, including xanthine oxidase (XOD) inhibitors and uricosuric agents, have adverse effects such as hepatic or renal toxicity and allergic reactions [3]. Therefore, exploration of safer and more effective therapeutic alternatives from traditional medicine holds substantial clinical significance.

P. umbellatus (Pers.) Fries, indigenous to China and utilized in traditional medicine, is a widespread sclerotial mushroom with therapeutic applications [4]. The dried sclerotium of *P. umbellatus*, known as Zhuling, has traditionally been used as a diuretic and dampness-eliminating agent. Modern pharmacological studies have demonstrated its diuretic, immunomodulatory, and antitumor activities [5,6]. However, systematic evaluation of *P. umbellatus* in the treatment of hyperuricemia, including its pharmacodynamic material basis and underlying molecular mechanisms remains lacking.

The current work was undertaken to: (i) examine whether PUE exerts hypouricemic, nephroprotective and anti-inflammatory activities in a chemically-induced murine model of HUA; (ii) identify the active fraction against HUA through bioactivity-guided fractionation; (iii) isolate and characterize the principal chemical constituents from the active fraction; and (iv) investigate the anti-inflammatory, antioxidant of the isolated compounds in monosodium urate (MSU)-stimulated RAW264.7 macrophages. This comprehensive approach aims to provide scientific evidence supporting the development and clinical application of *P. umbellatus* for the treatment of HUA.

2. Materials and Methods

2.1 Materials and Reagents

The dried sclerotia of *P. umbellatus* were bought from Bozhou Traditional Chinese Medicine Market (Bozhou, China), identified by Associate Professor Bao Shuyun from the College of Pharmacy of Wannan Medical University. A reference specimen (No. 20230612) was permanently maintained in the medicinal chemistry repository at the College of Pharmacy.

Experimental animals comprised male Kunming mice (SPF grade, 6–8 weeks) and ranging 20–24 g, were supplied by Henan Skbes Biotechnology Co., Ltd. (Henan, China). Prior ethical authorization was obtained from the Wannan Medical College Ethics Committee (Approval No. WNMC-AWE-2023476) for all animal studies, which were carried out adhering to rigorous protocols ensuring humane treatment and proper utilization of laboratory animals. The study was carried out in accordance with the ARRIVE guidelines and Laboratory animal-Guideline for ethical review of animal welfare (GB/T 358922018, China).

Hypoxanthine and potassium oxonate were got from Aladdin Biochemical Technology Co., Ltd. (Shanghai, China). The reference compounds benzbromarone and colchicine were obtained from Changzhou Kangpu Pharmaceutical Co., Ltd. (Changzhou, China) and Xishuangbanna Pharmaceutical Co., Ltd. (Xishuangbanna, China), respectively. Commercial assay kits for uric acid, creatinine, blood urea nitrogen, and XOD activity were obtained from Nanjing Jiancheng Bioengineering Institute (Nanjing, China). ELISA kits for OAT1, URAT1, TNF-α, and IL-6 were purchased from Suzhou Calvin Biotechnology Co., Ltd. (Suzhou, China) and Wuhan ABclonal Biotechnology Co., Ltd. (Wuhan, China).

The ^{13}C NMR spectra and ESI-MS were recorded on an AM-400 spectrometer (Bruker, Germany) and a Thermo Scientific QE plus mass spectrometer (Thermo Fisher Scientific, Waltham, MA, USA), respectively. Their operating parameters can be found in the **Supplementary Material**.

2.2 Preparation of Polyporus umbellatus Extract (PUE)

For PUE preparation, 4400 g of dried sclerotia were extracted twice with 10 volumes of 95% ethanol (v/w) under reflux for 2 h each time. Pooled filtrates from the twin extractions were vacuum-concentrated and lyophilized, furnishing the crude PUE (508 g).

2.3 Fractionation of PUE by Macroporous Resin Chromatography

PUE (60 g) was dissolved in 95% ethanol and subjected to column chromatography using a D101 macroporous resin column. Elution was performed stepwise with distilled water followed by 30%, 70%, and 95% aqueous ethanol. The resulting four eluates were individually concentrated *in vacuo* and subjected to freeze-drying (each component weighing separately 0.6 g, 16 g, 35 g), resulting in four distinct powdered fractions for subsequent evaluation.

2.4 Animal Experimental Design

2.4.1 PUE Dose-Response Study

Following a 7-day environmental adaptation period, 60 male Kunming mice were allocated by randomization into six experimental cohorts (n = 10 animals per cohort): control, model, benzbromarone (7.5 mg/kg), PUE low-dose (105 mg/kg), PUE medium-dose (210 mg/kg), and PUE high-dose (420 mg/kg) groups. The dosage for the treatment group was calculated based on the weight of the freeze-dried extract relative to the original medicinal material. HUA was induced by intragastric administration of hypoxanthine (500 mg/kg) combined with intraperitoneal injection of potassium oxonate (250 mg/kg) daily for 14 days [7]. The interval between administration of the inducers and the test compounds was 1 h. Control mice received normal saline, while other groups received respective treatments.

2.4.2 Ethanol eluate Dose-Response Study

The 70 mice assigned to the evaluation of fraction efficacy were distributed across seven cohorts (n = 10 each): control, model, benzbromarone (7.5 mg/kg), 70% ethanol fraction at 29 and 115 mg/kg, and 95% ethanol fraction at 61 and 243 mg/kg.

2.5 Sample Collection and Biochemical Analysis

The main procedures were modified slightly from an earlier study [8]. After dosing, mice were immediately transferred to individual metabolic cages for the collection of urine specimens over a 24-h period. These were initially clarified by centrifugation (2000 rpm, 10 min), with the resulting supernatants immediately aliquoted and preserved at –80 °C pending quantification of UA. At the end of the experiment, mice were euthanized by intraperitoneal injection of sodium pentobarbital (50 mg/mL) at a dose of 150 mg/kg. Blood was then collected via retro-orbital puncture and allowed to clot at 4 °C for 4 h. Serum was isolated by centrifugation at 3500 rpm for 15 min.

Left kidney tissues were homogenized for Western blot and Real-time Quantitative Polymerase Chain Reaction (qPCR) analyses. Right kidneys were fixed in 4% paraformaldehyde for 7 days for histopathological examination. Serum and liver XOD activities were determined as described previously [9] using commercial assay kits.

2.6 Histopathological Examination

The histopathological assessment was conducted as described earlier [10]. Standard tissue processing was applied to kidney specimens, encompassing fixation, graded ethanol dehydration, and paraffin embedding. From these blocks, 4-μm serial sections were generated via rotary microtomy and subsequently processed for H&E staining to visualize tissue architecture. Morphological changes were

Table 1. Primer sequences for qRT-PCR.

Gene	Forward primer	Reverse primer
TNF-α	ACCCTCACACTCAGATCATCTTC	TGGTGGTTTGCTACGACGT
IL-6	CCAGTTGCCTTCTTGGGACT	CTGGTCTGTTGTGGGTGGTA
URAT1	CGCTTCCGACAACCTCAATG	CTTCTGCGCCCAAACCTATCT
OAT1	CACCTGCTAATGCCAACCTC	CCATTGTGCGGGAAAGGAAA
GAPDH	GAAGGTCGGTGTGAACGGAT	CCCATTTGATGTTAGCGGGAT

evaluated by light microscopy at 400× magnification following standard tissue processing.

2.7 Quantitative Real-Time PCR (qRT-PCR)

The experimental method was carried out with reference to the literature [11]. RAW264.7 cells were seeded in a 6-well culture plate at a density of 4×10^6 cells. Total RNA was isolated from snap-frozen renal cortex samples (50–100 mg) employing 1 mL of TRIzol™ Reagent (Invitrogen, Thermo Fisher Scientific, USA; Cat. No. 15596026). The tissue was homogenized, left on ice for 10 min, then mixed with 200 µL of chloroform, vortexed vigorously for 15 s, and incubated on ice for an additional 5 min. After centrifugation at 12,000 ×g for 15 min at 4 °C, the upper aqueous layer was collected, and RNA was precipitated by adding an equal volume of isopropanol and keeping the mixture at –20 °C for 30 min. The resultant pellet was rinsed with 75% ethanol and resuspended in 20 µL of DEPC-treated water. Purity and concentration were assessed with a NanoDrop™ One Spectrophotometer (Thermo Fisher Scientific), accepting A_{260}/A_{280} ratios between 1.8 and 2.1. For cDNA synthesis, the PrimeScript™ RT Reagent Kit with gDNA Eraser (Perfect Real Time) (Takara Bio Inc., China; Cat. No. RR047A) was used in a 20-µL reaction containing 1 µg of total RNA (≤8 µL), 1× RT Master Mix, 1 µL RT Enzyme Mix I, and 1 µL gDNA Eraser. The thermal profile on a T100 Thermal Cycler (Bio-Rad) comprised gDNA removal at 42 °C for 2 min, reverse transcription at 37 °C for 15 min, and termination at 85 °C for 5 s. The resulting cDNA was diluted 1:5 with nuclease-free water and stored at –20 °C. Real-time PCR was carried out with TB Green® Premix Ex Taq™ II (Tli RNaseH Plus) (Takara Bio; Cat. No. RR820A) supplemented with 50× ROX Reference Dye II, using a QuantStudio™ 5 system (Applied Biosystems). Each 20-µL reaction contained 10 µL of 2× Master Mix, 0.8 µL each of forward and reverse primers (10 µM stock, final 0.4 µM), 0.4 µL of 50× ROX dye, 2 µL of the 5-fold diluted cDNA, and 6 µL of water. The amplification protocol started with 95 °C for 30 s (one cycle), then 40 cycles of 95 °C for 5 s and 60 °C for 30 s (fluorescence reading), followed by a melting curve analysis from 60 °C to 95 °C with 0.5 °C steps every 5 s. Primers targeting the genes of interest (listed in Table 1) were obtained from Sangon Biotech Co., Ltd. (Shanghai, China), and GAPDH served as the endogenous control. Relative transcript levels were determined via the $2^{-\Delta\Delta Ct}$ method.

2.8 Western Blot Analysis

Immunoblotting was performed following established protocols [12,13]. Renal cortical tissues were homogenized in chilled RIPA buffer (Beyotime, Shanghai, China, #P0013B) containing 1 mM PMSF (Beyotime, #ST506) and a phosphatase inhibitor cocktail (Applygen, #P1081). After centrifugation, supernatants were collected and protein content determined using the BCA assay (Beyotime, #P0012) per the supplier's instructions. Equal amounts (40 µg per lane) of protein extracts were resolved on 10% SDS-polyacrylamide gels at 120 V for 90 min with running buffer (25 mM Tris, 192 mM glycine, 0.1% SDS, pH 8.3). Separated proteins were then transferred onto PVDF membranes (0.45 µm, Merck Millipore, Darmstadt, Germany, #ISEQ00010) via a semi-dry blotting apparatus (Bio-Rad Trans-Blot Turbo, Hercules, CA, USA) set at 25 V for 30 min, using transfer buffer (25 mM Tris, 192 mM glycine, 20% methanol, pH 8.3). To block non-specific binding, membranes were incubated for 1 h at ambient temperature with 5% (w/v) non-fat dry milk (Beyotime, #P0216) dissolved in TBST (20 mM Tris-HCl, 150 mM NaCl, 0.1% Tween-20, pH 7.6), under mild agitation. Next, blots were probed overnight at 4 °C (16 h) with primary antibodies: rabbit anti-URAT1 (1:1000, Affinity, #DF12340), rabbit anti-OAT1 (1:1000, Affinity, #DF6633), and rabbit anti-GAPDH (1:5000, Affinity, China, #AF7021) as the loading reference. Following three TBST washes (10 min each), the membranes were exposed to HRP-conjugated goat anti-rabbit IgG (1:5000, Affinity, #S0001) for 1 h at room temperature. Signal development used the ECL Plus substrate (Beyotime, #P0018S), and chemiluminescent images were acquired with the ChemiDoc XRS+ system (Bio-Rad). Densitometric quantification of band intensities was performed with ImageJ (v1.53, NIH, Bethesda, MD, USA), and each target protein signal was normalized to the corresponding GAPDH level.

2.9 Isolation of Major Compounds From the Active Fraction

Silica gel chromatographic separation of the 95% ethanol fraction (1.8 g) was performed by gradient elution with petroleum ether–EtOAc (20:1 → 4:1). This yielded three fractions, of which fraction 2 was crystallized to obtain compound A (160.8 mg), while fraction 3 was purified by semi-preparative HPLC (acetonitrile:water, 90:10, v/v) to obtain compound B (60.1 mg).

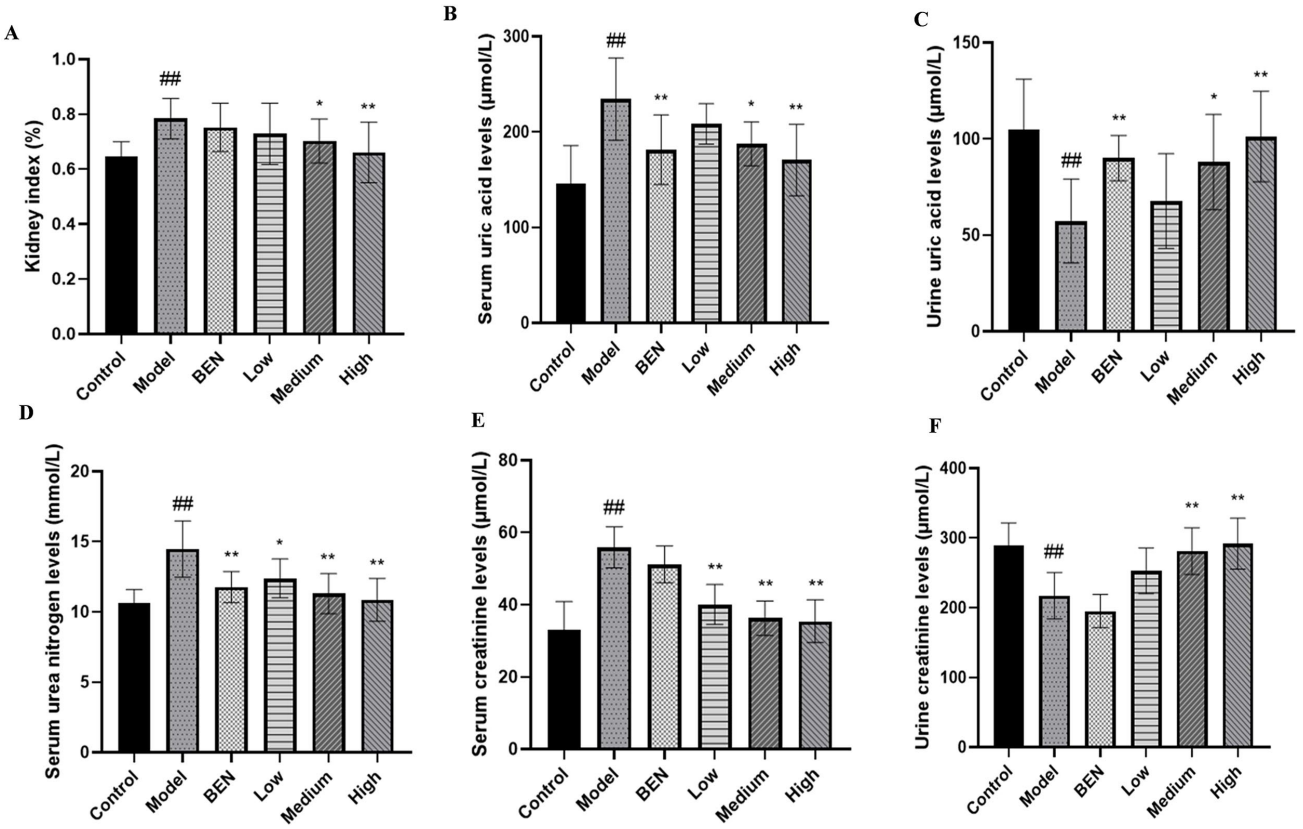

Fig. 1. Effects of PUE on renal function and uric acid metabolism in hyperuricemic mice. (A) Kidney index. (B) Serum uric acid. (C) Urinary uric acid. (D) Serum urea nitrogen. (E) Serum creatinine levels. (F) Urine creatinine levels. $^{\#\#}$ $p < 0.01$, * $p < 0.05$, ** $p < 0.01$. PUE, *Polyporus umbellatus* extract.

2.10 Molecular Docking Studies

Compounds A and B were docked to XOD (PDB: 1FIQ), URAT1 (homology model), and OAT1 (PDB: 6Q6C) using AutoDock Vina (v1.2.7, The Scripps Research Institute, USA). Proteins were prepared in AutoDockTools, ligands optimized with MM2 minimization. Grid box (60 × 60 × 60 Å) centered on active sites. Lamarckian Genetic Algorithm: 150 population, 2.5×10^6 evaluations, 100 runs. Binding energies (kcal/mol) and interaction residues were analyzed in PyMOL 2.5 (Schrödinger Inc., New York, NY, USA) [14].

2.11 Cell Culture and MSU-Induced Inflammation Model

Murine RAW264.7 macrophages were obtained from Procell Life Science & Technology (Wuhan, China) and maintained in DMEM supplemented with 10% FBS, 100 IU/mL penicillin G, and 100 μg/mL streptomycin sulfate. The cells were verified by STR typing and were found to be free of mycoplasma. Adhering to previously published methodologies [15], cells were incubated at 37 °C in a humidified 5% CO_2 atmosphere. For functional assays, cells were plated at 1×10^5 cells per well in 6-well dishes and allowed to attach for 16–18 h. Before pharmacological stimulation, the cells were kept in serum-free conditions (DMEM without FBS) for 12 h. Inflammatory conditions were subsequently established by exposure to MSU crystals for 24 h at 150 μg/mL.

2.12 Cell Viability Assay

The MTT assay was used to measure cell metabolic activity according to previously described methods [16,17]. The experimental protocol entailed seeding cells into 96-well microplates at 1×10^4 cells per well. After treatment, cells were incubated with MTT working solution (0.5 mg/mL, diluted from a 5 mg/mL stock) for 4 h at 37 °C. Subsequently, the formazan crystals formed were dissolved in DMSO for measurement. Optical density was determined spectrophotometrically at 490 nm or 550 nm using an automated microplate spectrophotometer.

2.13 Determination of Nitric Oxide (NO), MDA and SOD Levels

RAW264.7 cells were pretreated with MSU (150 μg/mL) for 24 h, followed by treatment with compounds A (100, 300 μg/mL) or B (5, 15 μg/mL) for 24 h. The supernatant was collected for NO measurement. Cells were lysed, and the lysates were analyzed for MDA content and SOD activity using commercial assay kits as described previously [18,19].

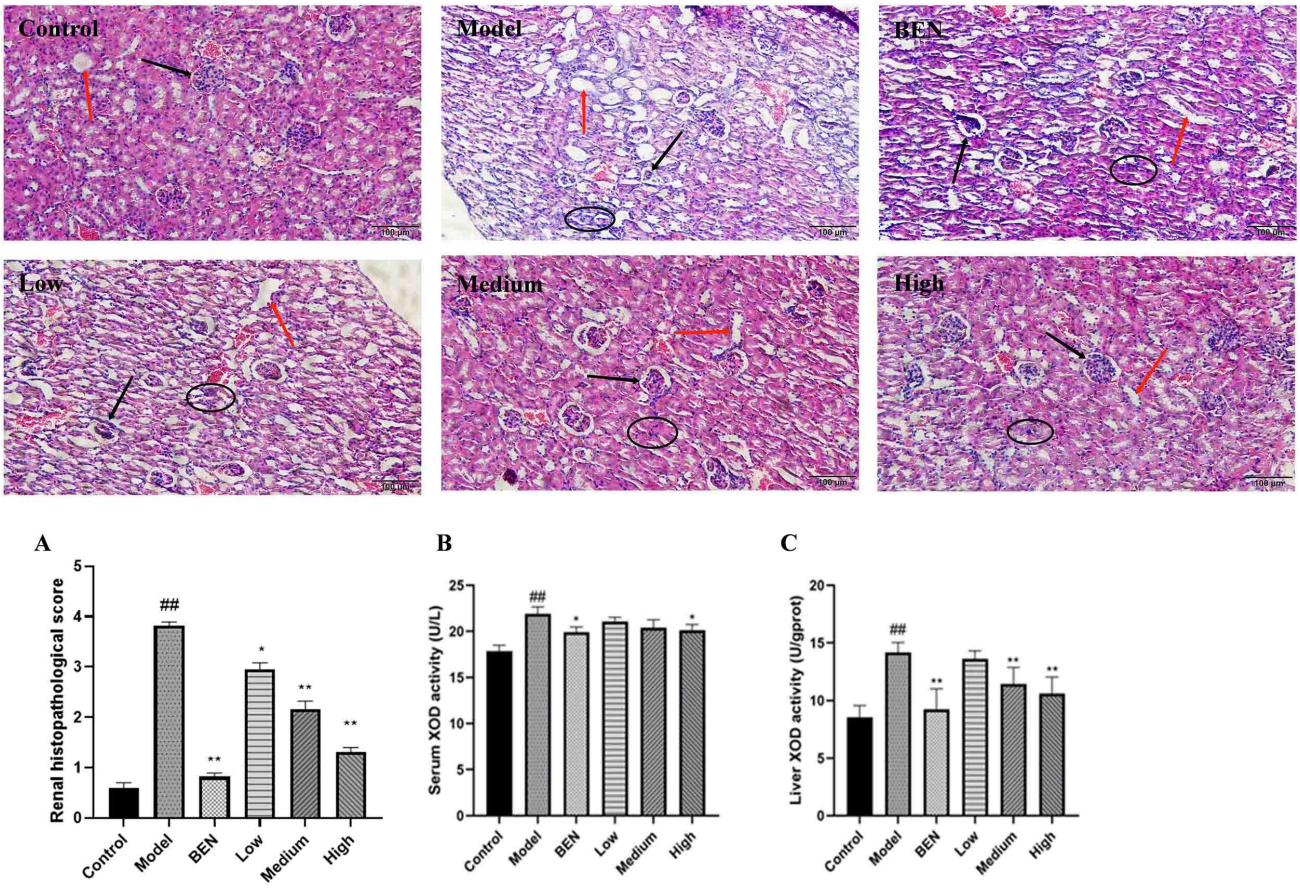

Fig. 2. Effects of PUE on xanthine oxidase activity and renal histopathology in hyperuricemic mice. (A) Renal histopathological scores. (B) Serum xanthine oxidase activity. (C) Hepatic xanthine oxidase activity. Representative H&E staining images (400× magnification): control, model, benzbromarone, PUE low-dose, PUE medium-dose, and PUE high-dose. Red arrow, renal tubule; black arrow, glomerulus; black circle, space between renal capsule and renal tubule. Scale bar = 100 μm. $^{\#\#}$ $p < 0.01$, * $p < 0.05$, ** $p < 0.01$. BEN, benzbromarone.

2.14 Statistical Analysis

All statistical analyses were performed with SPSS Statistics software (version 20.0, IBM Corp., Armonk, NY, USA). Quantitative data are expressed as the mean ± SD (n = 10). A two-tailed independent samples *t*-test was employed for dichotomous comparisons. One-way ANOVA was used for comparison of three or more groups, followed by post-hoc tests. Fisher's least significant difference (LSD) test was applied if the variance was homogeneous (as confirmed by Levene's test), while Dunnett's T3 procedure was used for heterogeneous variances. Statistical differences are indicated as compared with the control group ($^{\#}$ $p < 0.05$, $^{\#\#}$ $p < 0.01$) and the model (* $p < 0.05$, ** $p < 0.01$).

3. Results

3.1 Effects of Polyporus umbellatus Extract on Hyperuricemia and Renal Function in Mice

The effects of PUE on renal function and UA metabolism are presented in Fig. 1. HUA mice exhibited significantly elevated renal index, serum UA, creatinine (CRE), and blood urea nitrogen (BUN) levels, with reduced urinary UA excretion ($p < 0.01$), thus confirming successful establishment of the model. Treatment with PUE ameliorated these abnormalities in a dose-dependent manner: medium and high doses significantly reduced the renal index ($p < 0.05$ and $p < 0.01$), while all doses lowered serum UA and increased urinary UA excretion ($p < 0.05$ or $p < 0.01$). Notably, the positive control benzbromarone failed to improve the renal index despite lowering serum UA.

3.2 Effects of PUE on XOD Activity and Renal Histopathology in HUA Mice

PUE significantly inhibited XOD activity in both the serum and liver ($p < 0.01$, Fig. 2B,C). Histopathological examination revealed severe glomerular enlargement, tubular vacuolization, and inflammatory infiltration in HUA mice (Fig. 2, Model). These pathological lesions were obviously alleviated in both the benzbromarone (BEN) group and high-dose PUE group (Fig. 2, BEN and High). Quantitative assessment of renal histopathological scores further

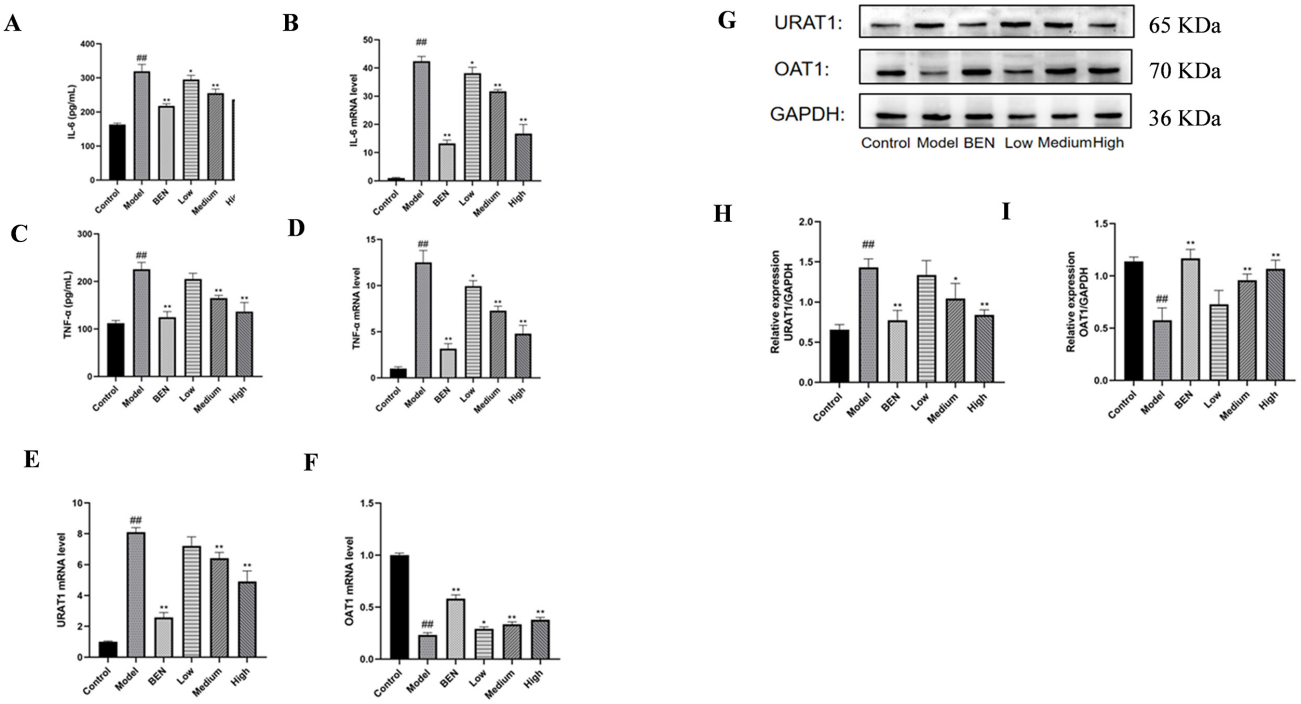

Fig. 3. Effects of PUE on inflammatory cytokines and renal urate transporters in hyperuricemic mice. (A) IL-6 levels. (B) *IL-6* mRNA level. (C) TNF-α levels. (D) *TNF-α* mRNA expression. (E) *URAT1* mRNA level. (F) *OAT1* mRNA level. (G) Representative Western blot of URAT1, OAT1, and GAPDH. (H) Quantification of URAT1 protein. (I) Quantification of OAT1 protein. $^{\#\#}$ $p < 0.01$, * $p < 0.05$, ** $p < 0.01$.

confirmed that PUE treatment significantly reduced kidney damage in a dose-dependent manner ($p < 0.01$, Fig. 2A).

3.3 Effects of PUE on Inflammatory Cytokines and Urate Transporters in Kidney Tissues

PUE significantly attenuated renal inflammation, reducing IL-6 and TNF-α expression at both protein and mRNA levels ($p < 0.05$ or $p < 0.01$, Fig. 3A–D). Furthermore, PUE modulated the expression of renal urate transporter, downregulating URAT1 and upregulating OAT1 at both the transcriptional and translational levels ($p < 0.01$, Fig. 3E–I).

3.4 Bioactivity-Guided Fractionation and Identification of the Active Fraction

To identify the active fraction of PUE, the extract was fractionated by D101 macroporous resin column chromatography. HPLC chromatograms of the ethanol extract and the fractions are shown in Fig. 4A. The 95% ethanol eluate demonstrated superior anti-HUA activity, significantly reducing the renal index, urinary uric acid, BUN, and CRE ($p < 0.05$ or $p < 0.01$, Fig. 4B–E). In contrast, the 70% ethanol eluate showed only marginal effects.

3.5 Comparison of the 70% and 95% Ethanol Eluates on XOD, Histopathology, and Inflammation

The 95% ethanol eluate significantly inhibited XOD activity in both the serum and liver at both doses ($p < 0.01$, Fig. 5F,G), whereas the 70% ethanol eluate only reduced liver XOD at the high dose ($p < 0.05$). Histopathological results showed that the 95% ethanol eluate markedly ameliorated renal damage, whereas the 70% ethanol eluate showed little improvement (Fig. 5, 95%-L and 95%-H vs. 70%-L and 70%-H). Quantitative assessment of renal histopathological scores further confirmed that the 95% ethanol eluate significantly reduced kidney damage in a dose-dependent manner ($p < 0.01$, Fig. 5A). The 95% ethanol eluate also significantly decreased both the protein levels and mRNA expression levels of IL-6 and TNF-α ($p < 0.05$ or $p < 0.01$, Fig. 5B–E).

3.6 Effects of the Active Fractions on Renal Urate Transporters

The modulation of renal urate transporters by the 70% and 95% ethanol eluates was assessed by qRT-PCR and Western blot (Fig. 6). HUA mice showed significantly increased expression of URAT1 mRNA and protein ($p < 0.01$) and decreased expression of OAT1 mRNA and protein ($p < 0.01$) compared to controls.

The 95% ethanol eluate at both low and high doses significantly downregulated URAT1 mRNA (Fig. 6A) and protein (Fig. 6D), and upregulated OAT1 mRNA (Fig. 6B) and protein (Fig. 6E) ($p < 0.01$). The 70% ethanol eluate reduced URAT1 mRNA at both doses ($p < 0.05$ or $p < 0.01$) and URAT1 protein at high dose ($p < 0.01$), but increased OAT1 mRNA and protein only at the high dose ($p < 0.05$).

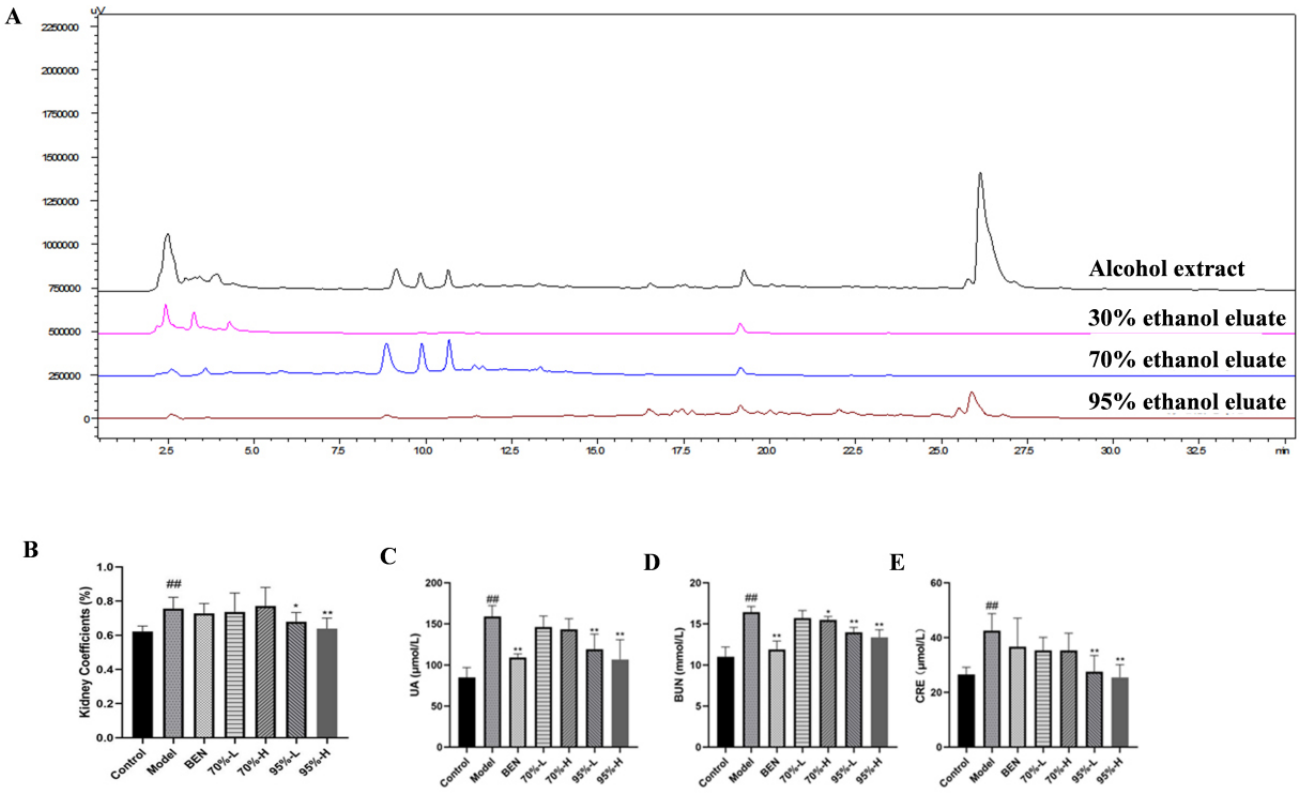

Fig. 4. Bioactivity-guided fractionation of *Polyporus umbellatus* extract (PUE) by D101 macroporous resin chromatography and evaluation of the eluates on renal function in hyperuricemic mice. (A) HPLC chromatograms of the ethanol extract and the fractions. (B) Kidney coefficients. (C) Urinary uric acid (UAC) levels. (D) Blood urea nitrogen (BUN) levels. (E) Creatinine (CRE) levels. $^{\#\#}p < 0.01$, $^{*}p < 0.05$, $^{**}p < 0.01$.

Representative Western blots are shown in Fig. 6C. These data demonstrate that the 95% ethanol eluate more effectively modulates urate transporters to promote the excretion of UA.

3.7 Identification of the Compounds

Two major compounds were isolated from the 95% ethanol eluate and identified. Their chemical structures are presented in Fig. 7A. Their HPLC chromatograms could be found in the **Supplementary Material**.

Compound A: White crystals. ESI-MS (m/s): 395[M–H]$^{-}$. Compound B: White powder. ESI- MS (m/s): 427[M–H]$^{-}$. Their ^{13}C-NMR spectrum data are shown in Table 2.

3.8 Chemical Structures of Isolated Compounds and Their Cytotoxicity in RAW264.7 Cells

The cytotoxicity of MSU and the compounds on RAW264.7 macrophages was evaluated by MTT assay (Fig. 7B–F). As shown in Fig. 7B, MSU at concentrations below 200 μg/mL had no significant cytotoxicity; therefore, 150 μg/mL MSU was selected for subsequent experiments. Compound A was non-toxic up to 300 μg/mL (Fig. 7C), and compound B was non-toxic up to 15 μg/mL (Fig. 7D) in normal RAW264.7 cells. In MSU-induced cells (Fig. 7E,F), compound A remained non-toxic up to 300 μg/mL, and compound B up to 15 μg/mL. Based on these results, concentrations of 100 and 300 μg/mL for compound A and 5 and 15 μg/mL for compound B were chosen for further studies.

Compound B exhibited stronger binding affinities than A to all three targets: XOD (–8.4 vs –7.2 kcal/mol), TNF (–9.73 vs –9.5 kcal/mol), and IL-6 (–8.92 vs –8.3 kcal/mol). Compound B formed hydrogen bonds with XOD catalytic residues (Arg233, Glu23) and π–π stacking with IL-6 Phe37/40. The enhanced polar interactions explain its superior activity (Fig. 7G).

3.9 Anti-Inflammatory, Antioxidant, and Transporter-Modulating Effects of Compounds A and B in MSU-Induced RAW264.7 Cells

In MSU-stimulated RAW264.7 macrophages, both compounds suppressed NO release and the expression of pro-inflammatory cytokines (IL-6, TNF-α, IL-1β) in a dose-dependent manner ($p < 0.05$ or $p < 0.01$, Fig. 8A–D). Both compounds reduced MDA levels and increased SOD activity ($p < 0.05$ or $p < 0.01$, Fig. 8E,F).

4. Discussion

UA is the final product of purine metabolism in humans, and the imbalance between its production and excre-

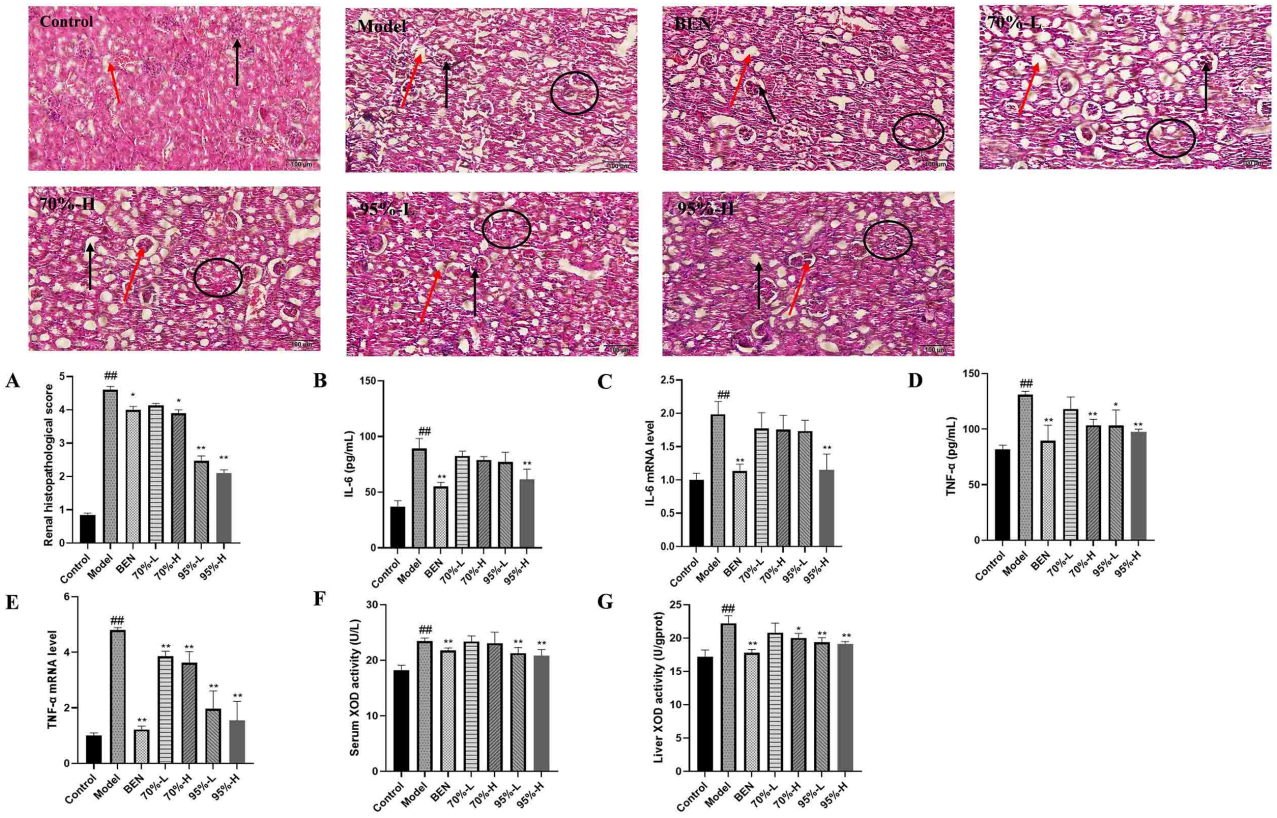

Fig. 5. Effects of 70% and 95% ethanol eluates on xanthine oxidase activity, renal histopathology, and inflammatory cytokines in hyperuricemic mice. (A) Renal histopathological scores. (B) IL-6 levels. (C) *IL-6* mRNA levels. (D) TNF-α levels. (E) *TNF-α* mRNA level. (F) Serum xanthine oxidase activity. (G) Hepatic xanthine oxidase activity. Representative H&E staining images (400× magnification): control, model, BEN, 70% ethanol fraction low-dose, 70% ethanol fraction high-dose, 95% ethanol fraction low-dose, and 95% ethanolfraction high-dose. Red arrow, renal tubule; black arrow, glomerulus; black circle, space between renal capsule and renal tubule. Scale bar = 100 μm. $^{\#\#}$ $p < 0.01$, * $p < 0.05$, ** $p < 0.01$.

Table 2. The ^{13}C-NMR (100 MHz) data of the two compounds in $CDCl_3$.

Position	Compound A (δ C)	Compound B (δ C)	Position	Compound A (δ C)	Compound B (δ C)
1	38.2	34.7	15	23.2	23.4
2	28.4	30.1	16	28.5	28.6
3	70.7	66.4	17	56.0	56.2
4	39.3	39.3	18	12.3	12.9
5	139.9	82.2	19	16.6	18.2
6	119.8	135.4	20	40.6	39.7
7	116.3	130.7	21	21.2	20.9
8	141.5	79.4	22	135.8	135.2
9	46.4	51.7	23	132.3	132.3
10	37.1	37.0	24	43.1	42.8
11	21.1	20.6	25	33.4	33.1
12	33.2	36.9	26	20.3	19.6
13	43.0	44.6	27	19.8	20
14	54.7	51.1	28	17.7	17.6

tion is the core pathogenesis of HUA and gout [20]. In the present study, successful establishment of the HUA mouse model was confirmed by significantly elevated serum UA and reduced urinary UA levels compared to the control group.

PUE demonstrated a significant uric acid-lowering effect in a dose-dependent manner, as evidenced by decreased serum UA and increased urinary UA levels, suggesting enhanced UA excretion. Additionally, PUE inhibited XOD activity, thereby reducing *de novo* UA synthesis. XOD-

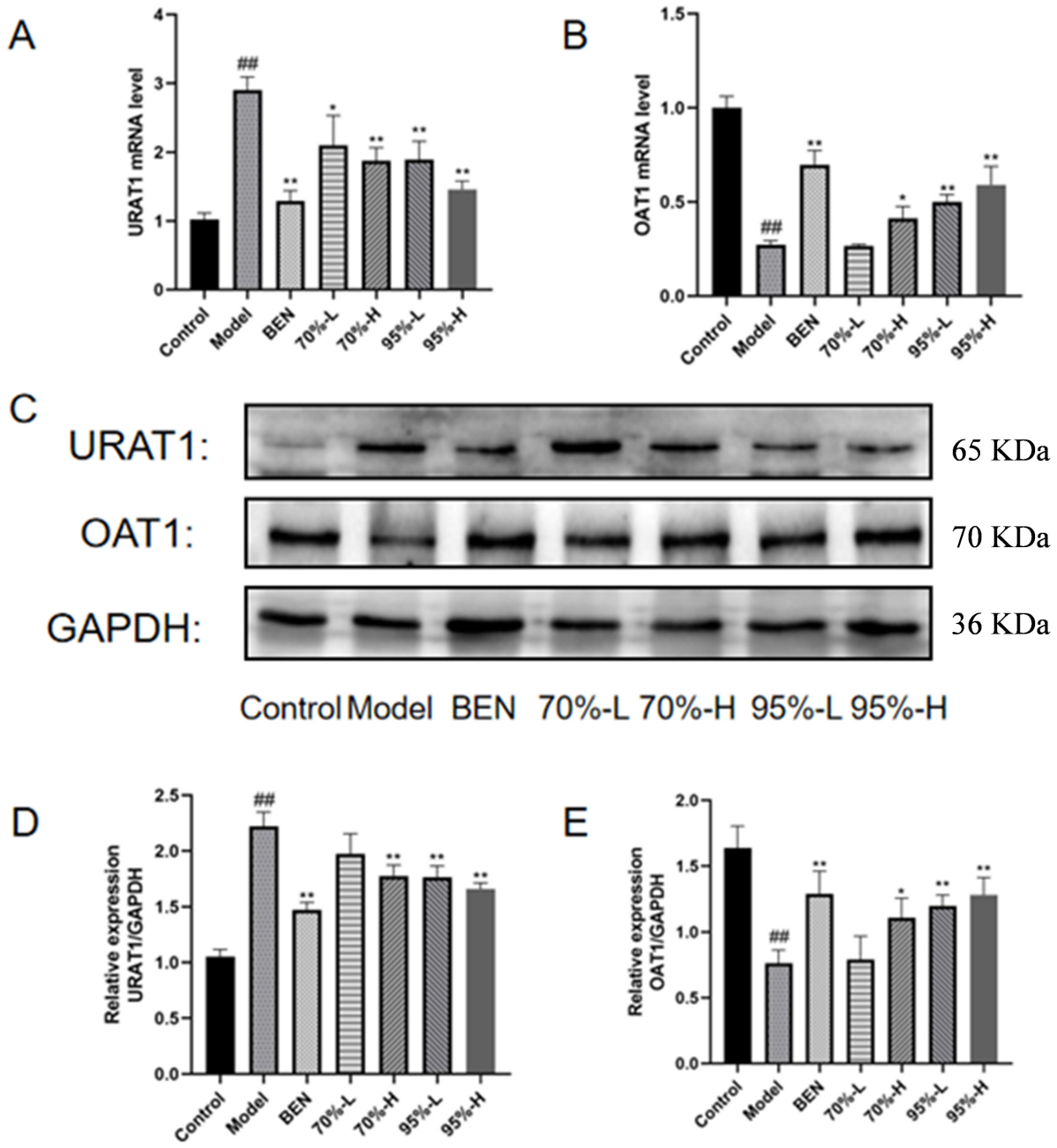

Fig. 6. Effects of 70% and 95% ethanol eluates on renal urate transporter expression in hyperuricemic mice. (A) *URAT1* mRNA expression. (B) *OAT1* mRNA expression. (C) Representative Western blot of URAT1, OAT1, and GAPDH. (D) Quantification of URAT1 protein. (E) Quantification of OAT1 protein. $^{\#\#}$ $p < 0.01$, * $p < 0.05$, ** $p < 0.01$.

mediated generation of reactive oxygen species (ROS) contributes to the activation of inflammatory signaling and renal oxidative damage [21,22], suggesting that XOD inhibition by PUE may confer dual benefits.

The kidney plays a pivotal role in UA homeostasis, with URAT1 and OAT1 serving as critical membrane transporters [23]. URAT1 facilitates UA reabsorption [24], while OAT1 promotes UA secretion into tubular fluid [25,26]. Our findings demonstrate that PUE significantly downregulates URAT1 expression while upregulating OAT1 expression, thereby promoting the net excretion of UA. This finding is consistent with reports on *Smilax china* L., which demonstrated the anti- hyperuricemia effect in animal models [27].

Importantly, PUE exhibited nephroprotective properties, as evidenced by reduced serum creatinine and blood urea nitrogen levels, as well as ameliorating renal histopathological changes. The nephroprotective effects of PUE may involve mechanisms analogous to those reported for betaine supplementation, which protects against high-fructose-induced renal injury through modulation of oxidative stress and inflammatory pathways [28].

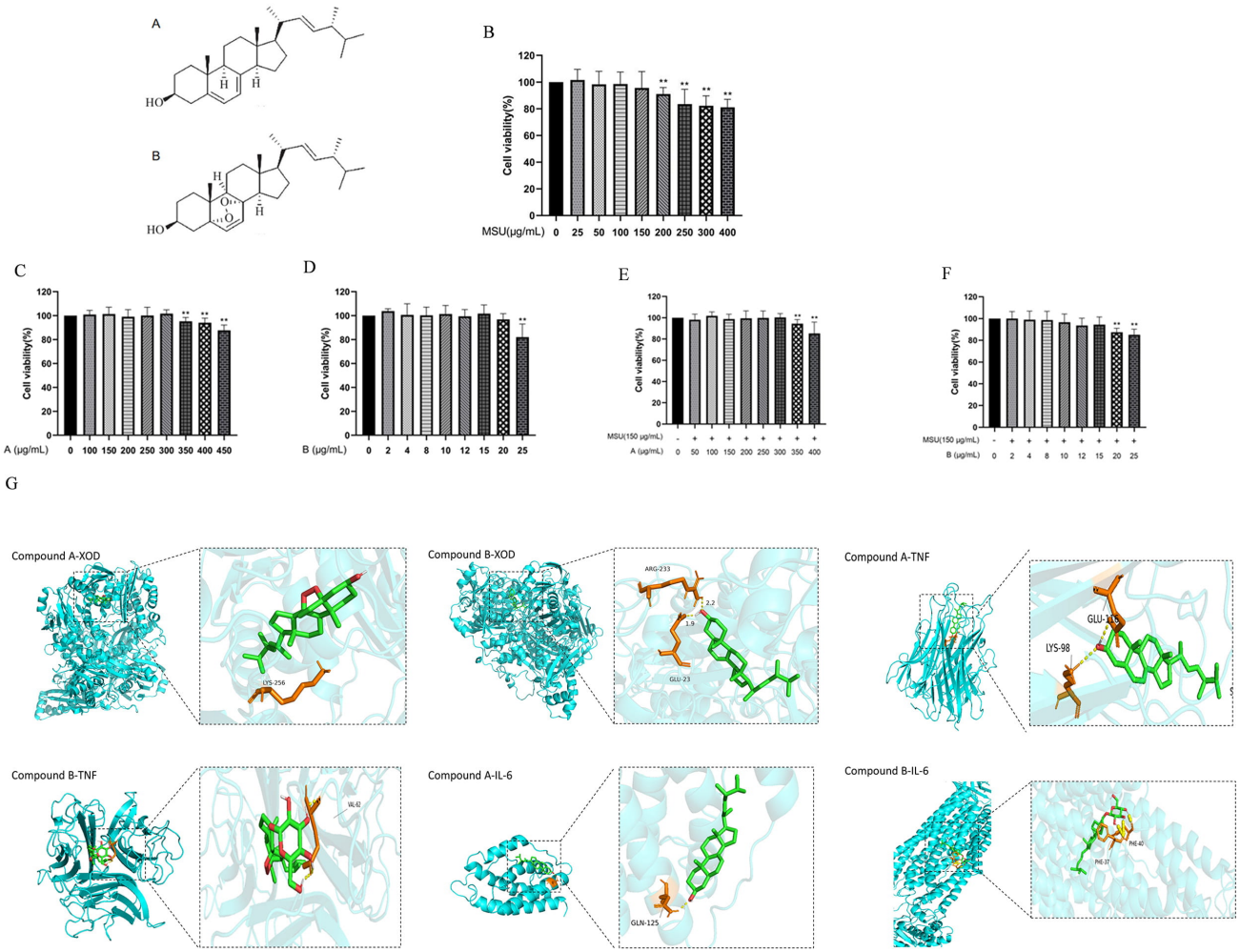

Fig. 7. Chemical structures, cytotoxicity of compounds A and B in RAW264.7 macrophages and molecular docking poses. (A) Chemical structures of the two compounds. (B) Cell viability of RAW264.7 cells treated with MSU. (C) Cell viability of RAW264.7 cells treated with compound A. (D) Cell viability of RAW264.7 cells treated with compound B. (E) Cell viability of MSU-induced RAW264.7 cells treated with compound A. (F) Cell viability of MSU-induced RAW264.7 cells treated with compound B. (G) Molecular docking poses of compounds A and B with xanthine oxidase (PDB: 1FIQ), TNF (PDB: 1TNF), and IL-6 (PDB: 1ALU). ** $p < 0.01$. MSU, monosodium urate; PDB, Protein Data Bank.

Persistent HUA represents a significant risk factor not only for chronic kidney disease but also for cardiovascular diseases, hypertension, and related complications [29], highlighting the clinical importance of strategies for reducing uric acid levels.

PUE significantly attenuated renal inflammation by suppressing pro-inflammatory cytokine production. Inflammatory cytokines, including TNF-α and IL-6, play crucial roles in hyperuricemia and related concurrent kidney diseases [30,31]. Elevated IL-6 levels have been shown to predict kidney disease progression in diabetic nephropathy and other renal conditions [32], highlighting the clinical relevance of IL-6 suppression in HUA management.

Bioactivity-guided fractionation identified the 95% ethanol eluate as the most potent fraction, exhibiting superior anti-hypouricemic, nephroprotective, XOD inhibitory, and anti-inflammatory activities compared to the 70% ethanol eluate. Chemical investigation of this active fraction led to the isolation of two ergosterol derivatives.

Molecular docking revealed that the 5α,8α-epidioxy bridge of compound B conferred superior binding to XOD, URAT1, and OAT1 compared to ergosterol (compound A). The enhanced hydrogen bond network and π-π stacking interactions correlate with the potent XOD inhibition and transporter modulation observed experimentally. These two main compounds isolated from the 95% ethanol eluate act as potential uric acid-lowering active molecules, and their effects are related to the inhibition of XOD activity and the increase in transporter expression.

The *in vitro* experiments in the current study were designed to further verify the anti-inflammatory effects of these two compounds. Acute gouty arthritis is triggered by MSU crystal deposition in joints, inducing inflammatory cytokine production [33]. Both compounds A and B

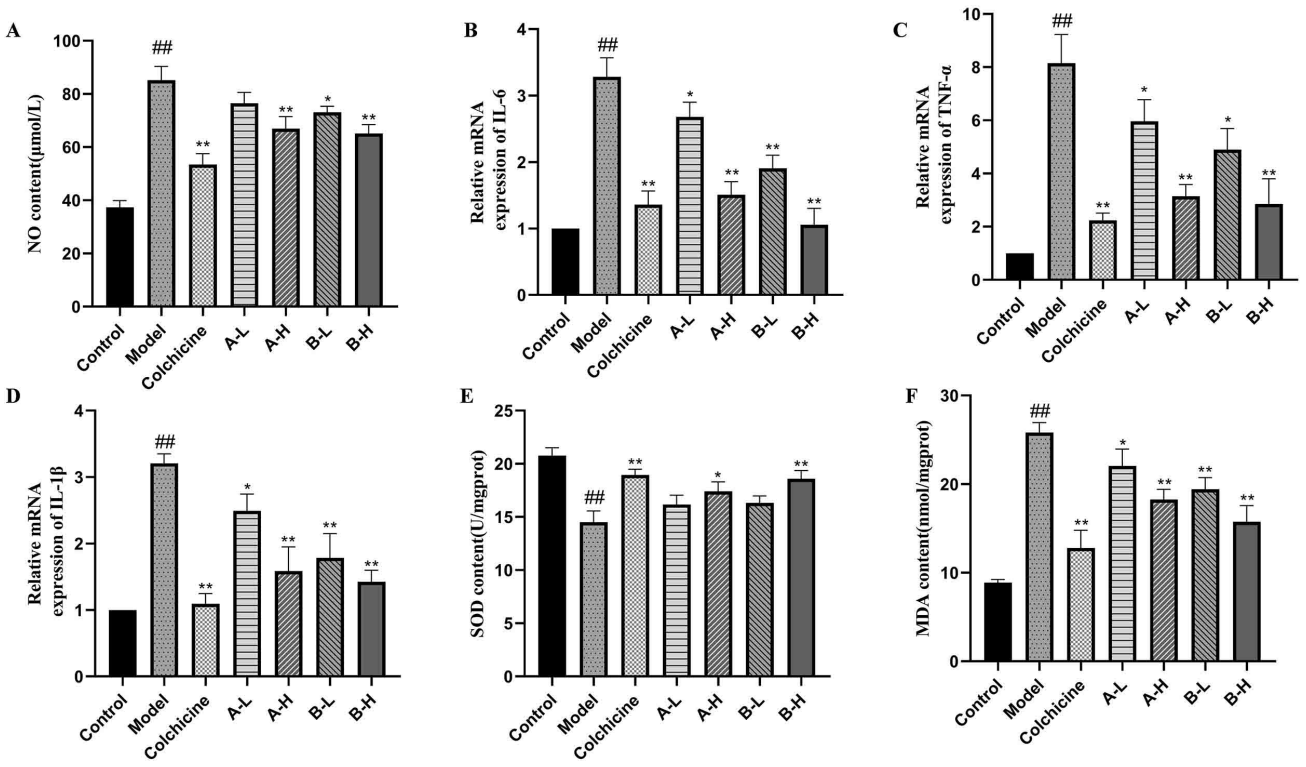

Fig. 8. Effects of compounds A and B on inflammatory mediators and oxidative stress markers in MSU-induced RAW264.7 macrophages. (A) Nitric oxide (NO) concentration in cell culture supernatant. (B–D) Relative mRNA expression of pro-inflammatory cytokines IL-6, TNF-α, and IL-1β, respectively. (E) SOD Content. (F) MDA levels. $^{\#\#}p < 0.01$, $^{*}p < 0.05$, $^{**}p < 0.01$. SOD, superoxide dismutase; MDA, malondialdehyde.

effectively suppressed MSU-induced macrophage activation, thereby reducing NO release and pro-inflammatory cytokine expression (IL-6, TNF-α, IL-1β), and ameliorating oxidative stress. Research on traditional Chinese medicine compounds for treating the gouty arthritis has demonstrated multiple mechanisms, including suppression of the NLRP3/ASC/Caspase-1 axis [34] and the regulation of pyroptosis pathways [35]. The anti-inflammatory action of ergosterol derivatives observed here suggests potential for alleviating acute gouty arthritis through the suppression of macrophage activation.

It has been reported that expression of the UA secretion and transport protein ABCG2 increased when HUA mice were treated with ergosterol, while expression of the UA reabsorption and transport protein GLUT9 significantly decreased, thereby reducing the accumulation of UA [36]. The two main active components in the 95% ethanol eluate of *P. umbellatus* are both ergosterol substances, with similar structures and binding ability to their corresponding targets. The similar molecular docking binding energies and similar binding modes of the two compounds also provide supportive evidence. Therefore, we propose that these two ergosterol derivatives are the potential molecules of *P. umbellatus* in the treatment of HUA.

5. Limitations

This study initially identified the active fraction of *P. umbellatus* in the treatment of hyperuricemia, and hypothesized that the possible effective components might be ergosterol derivatives. It is necessary to further confirm the effects of the active ingredients through *in vivo* and *in vitro* experiments and clarify their specific mechanisms.

Given that the active fraction reduces uric acid while also having anti-inflammatory effects, more in-depth research should be conducted on gouty arthritis caused by high uric acid levels in the later stage of hyperuricemia.

6. Conclusion

Polyporus umbellatus ethanol extract, particularly the 95% ethanol fraction containing ergosterol derivatives, may exert anti-hyperuricemia and its associated complications through multiple pathways: inhibition of uric acid synthesis (XOD inhibition), promotion of uric acid excretion (URAT1 downregulation and OAT1 upregulation), anti-inflammatory activity, and antioxidant protection. These findings support the potential clinical application of *P. umbellatus* against hyperuricemia.

Availability of Data and Materials

The datasets used and analyzed during the current study are available from the corresponding authors on reasonable request.

Author Contributions

SN and LZ conceived and designed the study. JL, XC, RJ, SZ, MZ, DY, XG, and JX performed the experiments. YC and YS analyzed the data. JL and XC drafted the manuscript. SN and LZ revised the manuscript critically for important intellectual content. All authors contributed to editorial changes in the manuscript. All authors read and approved the final manuscript. All authors have participated sufficiently in the work and agreed to be accountable for all aspects of the work.

Ethics Approval and Consent to Participate

All animal experimental procedures were approved by the Ethics Committee of Wannan Medical College (Approval No. WNMC-AWE-2023476). The study was carried out in accordance with the Laboratory Animal Guideline for ethical review of animal welfare (GB/T 358922018, China). The study was carried out in accordance with the ARRIVE guidelines.

Acknowledgment

Thanks for the equipment support provided by the Provincial Engineering Laboratory for Screening and Revaluation of Active Compounds of Herbal Medicines in Southern Anhui. Thank the Scientific Compass for conducting the spectral data test.

Funding

This work was supported by the Project of Xin'an Medicine and Modernization of Traditional Chinese Medicine Research Institute (No. 2023CXMMTCM007), Key Projects of Scientific Research in Higher Education Institutions of Anhui Province (KJ2020A0608), Anhui Provincial University STEM Faculty Enterprise Secondment and Practical Training Program Project (2025jsqygz39), Anhui Provincial Key Scientific Research Project Foundation (2025AHGXZK30634), Anhui Provincial Cultivation Project for Outstanding Young Teachers (YQYB2024046).

Conflicts of Interest

The authors declare that they have no competing interests. Although technical support was received from Scientific Compass, the interpretation of the data and the writing of the manuscript were not influenced by this relationship.

Supplementary Material

Supplementary material associated with this article can be found, in the online version, at https://doi.org/10.31083/Pharmazie54200.

References

[1] Li X, Chen Z, Zhang Y, Fan C, Chen L, Xu X, et al. Research progress on multidimensional intervention strategies for hyperuricemia: Western medicine, Traditional Chinese Medicine, and emerging therapies. Frontiers in Endocrinology. 2025; 16: 1722245. https://doi.org/10.3389/fendo.2025.1722245

[2] Zhou H, Yang J, Yuan X, Song X, Zhang X, Cao T, et al. Hyperuricemia research progress in model construction and traditional Chinese medicine interventions. Frontiers in Pharmacology. 2024; 15: 1294755. https://doi.org/10.3389/fphar.2024.1294755

[3] Major TJ, Dalbeth N, Stahl EA, Merriman TR. An update on the genetics of hyperuricaemia and gout. Nature Reviews. Rheumatology. 2018; 14: 341–353. https://doi.org/10.1038/s41584-018-0004-x

[4] Chinese Pharmacopoeia Commission. Pharmacopoeia of the People's Republic of China (Part 1). China Medical Science Press: Beijing. 2020.

[5] Ren S, Liu H, Sang Q, Sun Y, Li L, Chen W. *Polyporus umbellatus*, A Precious Rare Fungus With Good Pharmaceutical and Food Value. Engineering in Life Sciences. 2025; 25: e202400048. https://doi.org/10.1002/elsc.202400048

[6] Liu GK, Yang TX, Wang JR. Polysaccharides from Polyporus umbellatus: A review on their extraction, modification, structure, and bioactivities. International Journal of Biological Macromolecules. 2021; 189: 124–134. https://doi.org/10.1016/j.ijbiomac.2021.08.101

[7] Wu P, Li J, Zhang X, Zeng F, Liu Y, Sun W. Study of the Treatment Effects of Compound Tufuling Granules in Hyperuricemic Rats Using Serum Metabolomics. Evidence-based Complementary and Alternative Medicine: ECAM. 2018; 2018: 3458185. https://doi.org/10.1155/2018/3458185

[8] Zhang Y, Wang S, Dai X, Liu T, Liu Y, Shi H, et al. Simiao San alleviates hyperuricemia and kidney inflammation by inhibiting NLRP3 inflammasome and JAK2/STAT3 signaling in hyperuricemia mice. Journal of Ethnopharmacology. 2023; 312: 116530. https://doi.org/10.1016/j.jep.2023.116530

[9] Zhou LY, Peng JL, Wang JM, Geng YY, Zuo ZL, Hua Y. Structure-Activity Relationship of Xanthones as Inhibitors of Xanthine Oxidase. Molecules (Basel, Switzerland). 2018; 23: 365. https://doi.org/10.3390/molecules23020365

[10] Shen XB, Ding DL, Yu LZ, Ni JZ, Liu Y, Wang W, et al. Total extract of Anemarrhenae Rhizoma attenuates bleomycin-induced pulmonary fibrosis in rats. Bioorganic Chemistry. 2022; 119: 105546. https://doi.org/10.1016/j.bioorg.2021.105546

[11] Jin R, Zhao Z, Zhang Q, Sun YU, Wang W, Peng D, et al. An anti-inflammatory active ingredients in *Poriae cutis*: Screening based on network pharmacology. Die Pharmazie. 2024; 79: 72–81. https://doi.org/10.1691/ph.2024.3647

[12] Song X, Wang W, Liu L, Zhao Z, Shen X, Zhou L, et al. *Poria cocos* Attenuated DSS-Induced Ulcerative Colitis via NF-κB Signaling Pathway and Regulating Gut Microbiota. Molecules (Basel, Switzerland). 2024; 29: 2154. https://doi.org/10.3390/molecules29092154

[13] Shen X, Zheng Y, Yang H, Liu L, Yu L, Zhang Y, et al. Combination Treatment of Timosaponin BII and Pirfenidone Attenuated Pulmonary Fibrosis Through Anti-Inflammatory and Anti-Fibrotic Process in Rodent Pulmonary Fibrosis Model and Cellular Epithelial-Mesenchymal Transition Model. Molecules (Basel, Switzerland). 2025; 30: 1821. https://doi.org/10.3390/molecules30081821

[14] Trott O, Olson AJ. AutoDock Vina: improving the speed and accuracy of docking with a new scoring function, efficient optimization, and multithreading. Journal of Computational Chemistry. 2010; 31: 455–461. https://doi.org/10.1002/jcc.21334

[15] Sun S, Zhang J, Li H, Du Y, Li S, Li A, et al. Anti-inflammatory activity of the water extract of Chloranthus serratus roots in LPS-stimulated RAW264.7 cells mediated by the Nrf2/HO-1, MAPK and NF-κB signaling pathways. Journal of Ethnopharmacology. 2021; 271: 113880. https://doi.org/10.1016/j.jep.2021.113880

[16] Li J, Qian W, Xu Y, Chen G, Wang G, Nie S, et al. Activation of RAW 264.7 cells by a polysaccharide isolated from Antarctic bacterium Pseudoaltermonas sp. S-5. Carbohydrate Polymers. 2015; 130: 97–103. https://doi.org/10.1016/j.carbpol.2015.04.070

[17] Wu Q, Chen J, Zheng X, Song J, Yin L, Guo H, et al. Kaempferol attenuates doxorubicin-induced renal tubular injury by inhibiting ROS/ASK1-mediated activation of the MAPK signaling pathway. Biomedicine & Pharmacotherapy = Biomedecine & Pharmacotherapie. 2023; 157: 114087. https://doi.org/10.1016/j.biopha.2022.114087

[18] Zhou P, Wang Z, Chen C, Famurewa AC, Olatunji OJ. Naringin ameliorates 5-fluorouracil elicited neurotoxicity by curtailing oxidative stress and iNOS/NF-κB/caspase-3 pathway. Open Chemistry. 2023; 21: 20230126. https://doi.org/10.1515/chem-2023-0126

[19] Lin M, Wang G, Li Y. Structure, rheology and antioxidant properties of a polysaccharide from Atractylodes macrocephala in Pan'an. Carbohydrate Research. 2025; 552: 109464. https://doi.org/10.1016/j.carres.2025.109464

[20] Zhu Y, Zhang R, Wei Y, Cai M, Ma Y, Gu R, et al. Rice peptide and collagen peptide prevented potassium oxonate-induced hyperuricemia and renal damage. Food Bioscience. 2021; 42: 101147. https://doi.org/10.1016/j.fbio.2021.101147

[21] Ahlawat J, Sharma M, Pundir CS. Advances in xanthine biosensors and sensors: A review. Enzyme and Microbial Technology. 2024; 174: 110377. https://doi.org/10.1016/j.enzmictec.2023.110377

[22] Battelli MG, Bortolotti M, Polito L, Bolognesi A. The role of xanthine oxidoreductase and uric acid in metabolic syndrome. Biochimica et Biophysica Acta. Molecular Basis of Disease. 2018; 1864: 2557–2565. https://doi.org/10.1016/j.bbadis.2018.05.003

[23] Yang Q, Xu S, Shi X, Pang J, Wu T, Zhan P. Urate transporters: Structural mechanisms and therapeutic opportunities in drug development. Acta Pharmaceutica Sinica. B. 2026; 16: 3243–3248. https://doi.org/10.1016/j.apsb.2026.01.037

[24] Novikov A, Fu Y, Huang W, Freeman B, Patel R, van Ginkel C, et al. SGLT2 inhibition and renal urate excretion: role of luminal glucose, GLUT9, and URAT1. American Journal of Physiology. Renal Physiology. 2019; 316: F173–F185. https://doi.org/10.1152/ajprenal.00462.2018

[25] Lee CT, Chang LC, Liu CW, Wu PF. Negative correlation between serum uric acid and kidney URAT1 mRNA expression caused by resveratrol in rats. Molecular Nutrition & Food Research. 2017; 61: 10.1002/mnfr.201601030. https://doi.org/10.1002/mnfr.201601030

[26] Han S, Wei R, Han D, Zhu J, Luo W, Ao W, et al. Hypouricemic Effects of Extracts from *Urtica hyperborea* Jacq. ex Wedd. in Hyperuricemia Mice through XOD, URAT1, and OAT1. BioMed Research International. 2020; 2020: 2968135. https://doi.org/10.1155/2020/2968135

[27] Chen L, Yin H, Lan Z, Ma S, Zhang C, Yang Z, et al. Anti-hyperuricemic and nephroprotective effects of Smilax china L. Journal of Ethnopharmacology. 2011; 135: 399–405. https://doi.org/10.1016/j.jep.2011.03.033

[28] Fan CY, Wang MX, Ge CX, Wang X, Li JM, Kong LD. Betaine supplementation protects against high-fructose-induced renal injury in rats. The Journal of Nutritional Biochemistry. 2014; 25: 353–362. https://doi.org/10.1016/j.jnutbio.2013.11.010

[29] Zoccali C, Mallamaci F. Uric acid, hypertension, and cardiovascular and renal complications. Current Hypertension Reports. 2013; 15: 531–537. https://doi.org/10.1007/s11906-013-0391-y

[30] Wellby ML, Kennedy JA, Pile K, True BS, Barreau P. Serum interleukin-6 and thyroid hormones in rheumatoid arthritis. Metabolism: Clinical and Experimental. 2001; 50: 463–467. https://doi.org/10.1053/meta.2001.21034

[31] Zhou Y, Fang L, Jiang L, Wen P, Cao H, He W, et al. Uric acid induces renal inflammation via activating tubular NF-κB signaling pathway. PloS One. 2012; 7: e39738. https://doi.org/10.1371/journal.pone.0039738

[32] Sanchez-Alamo B, Shabaka A, Cachofeiro V, Cases-Corona C, Fernandez-Juarez G, PRONEDI study investigators. Serum interleukin-6 levels predict kidney disease progression in diabetic nephropathy. Clinical Nephrology. 2022; 97: 1–9. https://doi.org/10.5414/CN110223

[33] Wang Y, Zhu W, Lu D, Zhang C, Wang Y. Tetrahydropalmatine attenuates MSU crystal-induced gouty arthritis by inhibiting ROS-mediated NLRP3 inflammasome activation. International Immunopharmacology. 2021; 100: 108107. https://doi.org/10.1016/j.intimp.2021.108107

[34] Zhang X, Liu Y, Deng G, Huang B, Kai G, Chen K, et al. A Purified Biflavonoid Extract From *Selaginella moellendorffii* Alleviates Gout Arthritis via NLRP3/ASC/Caspase-1 Axis Suppression. Frontiers in Pharmacology. 2021; 12: 676297. https://doi.org/10.3389/fphar.2021.676297

[35] Fu X, Hong W, Li S, Chen Z, Zhou W, Dai J, et al. Wood smoke particulate matter (WSPM2.5) induces pyroptosis through both Caspase-1/IL-1β/IL-18 and ATP/P2Y-dependent mechanisms in human bronchial epithelial cells. Chemosphere. 2022; 307: 135726. https://doi.org/10.1016/j.chemosphere.2022.135726

[36] Lang WY, Bao HY, Jia SH, Li JN, Wang X. Effects of Inonotus hispidus fruiting body extracts on reducing uric acid and protecting liver and kidney of hyperuricemia mice. Mycosystema. 2024; 43: 240072. https://doi.org/10.13346/j.mycosystema.240072